Engineered Science

Thermal Performance Improvement of Forced-Air Cooling System Combined with Liquid Spray for Densely Packed Batteries of Electric Vehicle

Patcharin Saechan,[1,*] Isares Dhuchakallaya,[2,*] and Fatimah Al Zahrah Mohd Saat[3]

Abstract

In the electric vehicles (EVs), battery thermal management system (BTMS) serves a key role in addressing the issue of excessive heat generated from chemical reactions and internal resistance which can cause capacity fade, thermal runaway and instability issues. In this study, a novel cooling system that combines liquid spray and forced-air is proposed. The cooling fluid used is Hydrofluoroether (HFE) which is a non-electrically conductive liquid. The study develops a transient heat transfer model of the battery module and investigates the effects of injection rate and injector arrangement on cooling performance. The results demonstrate that increasing the amount of HFE can further decrease the maximum temperature and the temperature non-uniformity of the battery module, but cost-benefit considerations must be taken into account. The injector layout also has a significant impact on the temperature distribution of the module. Optimizing the cooling system can reduce the maximum temperature and temperature difference of the module by 5.9 °C and 4.0 °C, respectively, compared to dry air cooling. These findings of the spray-assisted forced-air cooling system provide useful insights for developing a practical thermal management solution for EVs.

1. Introduction

The recent trend towards sustainable energy development aims to provide reliable energy supplies based on environmentally friendly principles and to promote affordable energy services as part of the United Nations' sustainable development goals. Fossil fuels are currently the main sources of energy consumption, but they are finite and contribute to greenhouse gas emissions. Clean energy and energy efficiency can reduce environmental impact and support sustainable development. In the transportation sector, electric vehicles (EVs) have become a popular choice as they produce no emissions and can be powered by renewable energy to create a more eco-friendly system. The EVs rely on batteries as their primary source of power. These batteries are connected in series/parallel to create a module, and multiple modules are combined to form a battery pack that can achieve the desired voltage and power capacity. The performance of the battery pack affects the overall performance, reliability, safety, and cost of the EVs. Lithium-ion batteries (LIBs) are the most commonly used type of battery for EVs due to their high energy density, low self-discharge rate, and long cycle life. However, their narrow optimum operating temperature range presents a challenge.

During charge and discharge periods, heat is generated inside the cells due to the electrochemical reactions. Appropriate heat removal is necessary to maximize battery power capacity and lifespan. If the battery cooling system fails to dissipate such heat, high temperatures inside the cells

[1] *Faculty of Engineering, King Mongkut's University of Technology North Bangkok, Bangsue, Bangkok, 10800, Thailand.*

[2] *Center of Excellence in Computational Mechanics and Medical Engineering, Thammasat School of Engineering, Faculty of Engineering, Thammasat University, Klong-Luang, Pathumthani, 12120, Thailand.*

[3] *Fakulti Kejuruteraan Mekanikal (FKM), Universiti Teknikal Malaysia Melaka (UTeM), Hang Tuah Jaya, Melaka, Durian Tunggal, 76100, Malaysia.*

Email: patcharin.s@eng.kmutnb.ac.th (P. Saechan); disares@engr.tu.ac.th (I. Dhuchakallaya)

reduce the internal resistance and result in self-discharge, irreversible chemical reactions, and shortened battery life. There is a growing body of literature that recognizes the importance of temperature on the performance of a battery. Most battery manufacturers recommend that the current LIB used in EVs typically require a reliable operating temperature range of -20 to 60 °C for operation. However, the recommended operating temperatures might be narrowed depending on the ambient temperature, rate of charge/discharge and ageing concern. Leng *et al*.[1] revealed that the temperature of a LIB increasing from 25 °C to 45 °C raised the degradation rate from 4.22% to 8.74%, and the degradation rate jumped to 13.24% at 55 °C. Additionally, the battery starts self-heating reaction due to the decomposition of solid electrolyte interface (SEI) film at temperature around 60–80 °C.[2] This exothermic decomposition of the SEI triggers the thermal runaway in the cell. To concern the life span and the safe operation under any conditions of LIBs, it is typically recommended to operate them within a temperature range of 25 to 40 °C.[3,4] An uneven temperature distribution in a battery pack can also affect battery performance, leading to unbalanced cells and reduced usable capacity. This circumstance increases internal resistance due to power losses.[5] An increase in temperature non-uniformity in the pack by 10–15 °C can reduce the capability of the LIBs by 30–50%.[6] To minimize this effect, temperature non-uniformity in the battery pack should be limited to less than 5 °C.[3] Therefore, the thermal impact and temperature uniformity of the battery pack are the main concerns for a battery thermal management system (BTMS) in EVs to ensure efficient and safe battery operation.

A variety of studies have been conducted on the BTMS to address temperature-related issues. These systems can be classified into three groups based on the working media used for heat dissipation: air, liquid, and phase change material (PCM). Each has its advantages and drawbacks. Air-based BTMSs are widely used due to their simplicity, cost-effectiveness, and reliability. The working fluid can be sourced from the atmosphere or the cabin. However, their performance is limited by factors such as low thermal capacity and temperature non-uniformity during high cooling loads. Recent studies report that natural convection can successfully dissipate heat in the battery pack operating at low discharge rates (0.5C). However, the air cooling is not adequate for thermal management at high discharge rates (2C).[7] This means that increasing the C-rate requires a larger amount of heat to be dissipated, where the C-rate indicates the number of hours a battery with a given capacity will last. Nowadays, the effectiveness of air-based BTMSs has been explored with

regards to air flow configuration,[8] cell arrangements,[9,10] and inlet/outlet configurations.[11] These systems have been applied in commercial EVs, such as Nissan Leaf and Toyota Prius.

The liquid-based cooling systems are more effective than air-cooled systems in dissipating heat in the battery pack. Liquid coolants have greater convective heat transfer coefficient, heat capacity, and thermal conductivity. There are two types of fluid used to dissipate heat in the battery pack: electrically conductive fluids, and non-electrically conductive fluids. Electrically conductive fluids, such as ethylene glycol, water, nanofluids, or the mixture of them, come into indirect contact with the batteries, which are placed in a fluid jacket,[12-14] to avoid reactions and corrosion. The convective boundary layer controls the cooling performance of this technique. The thermal resistances of the material layers sandwiched between the battery and the liquid coolant cause temperature gradients. These undesired resistances can be eliminated by soaking batteries in the liquid. However, this method has safety concerns related to short circuits in case of leakage. The commercial EV models, *i.e.*, GM Volt, Tesla model S, have implemented this innovated scheme as the cooling system. Non-electrically conductive fluids, such as mineral oil, silicone oil, and fluorinated hydrocarbon, are also used for entirely or partially submerged cooling, known as immersion cooling.[15,16] Typically, the thermal properties of non-electrically conductive fluids are inferior compared to common coolants like water. This method offers improved heat rejection rate and temperature uniformity. However, it is challenging to implement in practice due to extra weight, additional components, increased maintenance, and a need for more space.

The PCM-based approach utilizes a large heat capacity associated with a small change of temperature during the melting process of the materials to absorb the excess heat in the system. The heat is stored or released at a desirable melting temperature, and the latent heat of fusion is a key factor in achieving effective cooling.[17] PCMs have previously been used in cooling applications for electronics[18] and have recently gained interest due to their compactness, high efficiency, lightweight, low cost, and non-corrosive properties. However, the stored heat cannot be transferred directly from the PCM, so it is typically combined with other systems,[19-21] such as air cooling, liquid cooling, or heat pipes, to prevent heat buildup. Several attempts have been made to improve the cooling performance of the BTMS involving the PCM. Recently, the design of a battery cooling system employing various combination of PCM, metal foam and fins has been investigated.[22] This study indicated that the temperature of battery surface was kept at the lowest level under discharging

with 3C-rate and different environmental conditions. Moreover, the cooling performance of the LIBs was improved with the proposed methods.

Despite the success of the various cooling techniques for BTMS, they all have limitations. The optimum BTMS cannot be determined. Much uncertainty still exists regarding the current battery cooling techniques, presenting research opportunities for improvement in cooling performance. For liquid-based systems, the success of a direct cooling method depends on the convective heat transfer coefficients of the fluids. Most studies have been affected by the poor thermal properties of non-conductive liquids. Enhanced thermal management of the battery pack can be achieved by adding a small amount of non-electrically conductive coolant to the main airflow. The liquid is atomized into small droplets and vaporized into the airflow when absorbing heat from the surrounding air and battery surfaces to provide a cooling effect. The heat transfer coefficient is certainly improved due to a massive surface-area-to-volume ratio coupled with the broad dispersion of droplets across the battery surfaces. Two-phase flow of atomized coolant and air in a cooling system improves heat transfer rate compared to forced-air cooling alone, due to its high capability of dissipating heat.

Alkhedhair *et al.*[23] and Tissot *et al.*[24] conducted numerical studies to evaluate the impact of droplet size and air velocity on the cooling performance of heat exchangers through water sprays for pre-cooling of inlet air. They found that smaller droplets had a higher evaporation rate while higher air speed decreased the rate of droplet evaporation. Although larger droplets were less efficient for cooling, they had a greater dispersibility, leading to a more effective heat and mass exchange as a whole. To find the optimal condition by trading off between the effects of momentum exchange and evaporation rate, a balance must be considered between droplet size and air velocity. Montazeri *et al.*[25] analyzed the effect of physical parameters on the cooling performance of a water spray system and found that the cooling performance improved with a decrease in the mean droplet size. For a given mean droplet size, the cooling performance was enhanced for wider droplet-size distributions. The performance improvement of the air-cooled chiller with a water spray system was experimentally verified by Yang *et al.*[26]. The spray evaporative cooling system could reduce the power consumption of the compressor. The COP of the system increased by 4%–8%, corresponding to electricity-saving of 2.37%–13.53%. Yang *et al.*[27] investigated the use of water spray to pre-cool the inlet air for the BTMS. They found that an increase in water flow rate could decrease the maximum temperature of the battery, but caused a large temperature

distribution. Saw *et al.*[28] found that a water mist cooling system was capable of maintaining the battery temperature within the desired operating temperature range during 3C-rate charging. The potential of humid air cooling applications for battery packs was experimentally demonstrated by Zhao *et al.*[29] and Youssef *et al.*[30] The results indicated that the relative humidity of the ambient air had a significant effect on the cooling performance that ambient air with lower relative humidity provided better performance in heat dissipation. The evaporative cooling system was shown to improve the cooling efficiency of the battery with better temperature uniformity.

Although the cooling concept of the liquid spray on the hot battery surface has been explored for years, the applications of liquid spray cooling to the BTMS are rather new. Most recent research has not addressed the safety concerns for long-term usage as the atomized water is an electrically conductive fluid. Moreover, there are more hidden dangers caused by the fluid leakage or blockage. Integrating non-conductive liquid spray and forced-air cooling technology is crucial for improving the safety of Li-ion BTMS. The primary objective of this study is to investigate the potential of using non-electrically conductive liquid spray cooling to meet the temperature requirements for densely packed batteries. The positioning of the liquid jet is also examined to optimize the usage of liquid spray. The working liquid used in this research is hydrofluoroether (HFE) which has previously been used for immersion cooling in electronics[31] and battery cooling.[32,33] To date, however, there has been little convincing evidence to apply the HFE in two-phase evaporative LIB cooling application. This study aims to fill the research gaps and provide data on the viability of HFE in this technique.

2. Design of cooling system for battery module

Overall, it appears that batteries function effectively within a specific temperature range. The operating temperature should be kept in between 25 °C and 40 °C, while the temperature variation inside the battery pack should be less than 5 °C.[3,4] Most research efforts are focused on maintaining this optimal temperature range. In this study, a system consisting of both forced-air cooling and liquid spray cooling is proposed to dissipate heat from the EV battery. In order to operate an EV, a large amount of power is needed, which is achieved by connecting many thousands of battery cells. Simulating the heat transfer behavior of the entire battery pack used in the EV is not feasible due to limited simulation resources, therefore, this study focuses on examining a small battery module instead. As shown in Fig. 1, a battery module consisting of 40 cylindrical cells was placed in an air flow passage with a liquid spray arranged above the battery module to enhance the heat

dissipation of the cooling system. Commercial NCR18650B 3400-mAh Lithium Ion cells with NCA–LiNi$_{0.80}$Co$_{0.15}$Al$_{0.05}$O$_2$ cathode and graphite anode were used due to their higher specific energy and better cell uniformity. The cell components, including the positive electrode, negative electrode and separators are wound together into a jellyroll. The complex structure of cell components including jellyroll, current connectors, and safety devices was simplified by a homogeneous lump with an anisotropic thermal conductivity. The thermal properties of the cell could be determined based on the mass-weighted average of its constituents.[7] The thermo-physical properties of the cells are displayed in Table 1.

As seen in Fig. 1(a), the battery module was arranged in an inline layout with a center-to-center spacing of 21 mm in both the longitudinal and transverse directions. A uniform airflow rate of 2 m/s was induced at the inlet. To enhance the cooling performance, liquid droplets were atomized by an ultrasonic mist generator and injected through four solid-cone nozzles at the top of the domain. Each nozzle had an inner diameter of 1 mm. The liquid droplets injected were then suspended in the air stream to absorb heat from their surroundings. When the droplets impacted on the surface, they became deformed

partially by absorbing heat through conduction, eventually forming a thin liquid film. A significant amount of heat was removed by droplet impact, evaporation and liquid film convection. Moreover, the heat transfer was considerably improved in the droplet impingement zone. As such, the positioning of the nozzles, as shown in Fig. 1(b), should be optimized to attain high cooling performance.

Mudawar et al.[34] indicated that Novec fluid HFE-7100 is an ideal working fluid for direct-liquid-cooling systems in hybrid vehicles. It was evaluated based on environmental impact, thermophysical and dielectric properties, safety concerns, and material compatibility. Thus, HFE-7100 was chosen as the liquid coolant in this study. The properties of the test liquid 3M™ Novec™ Engineered Fluid HFE-7100 can be found in Table 2. It was noted that the liquid droplets and thin liquid film of HFE deposited on the cell surfaces could not be absorbed or diffuse into the cell materials; that could cause an adverse effect. In this study, after the Novec HFE-7100 fluid absorbs heat from the battery module, the idea of recirculating the fluid was considered. At the outlet of the battery cooling process, the fluid will have been heated and a considerable amount would have vaporized into gas-phase. To remove the HFE droplets from the hot air that is discharged outside, a mist
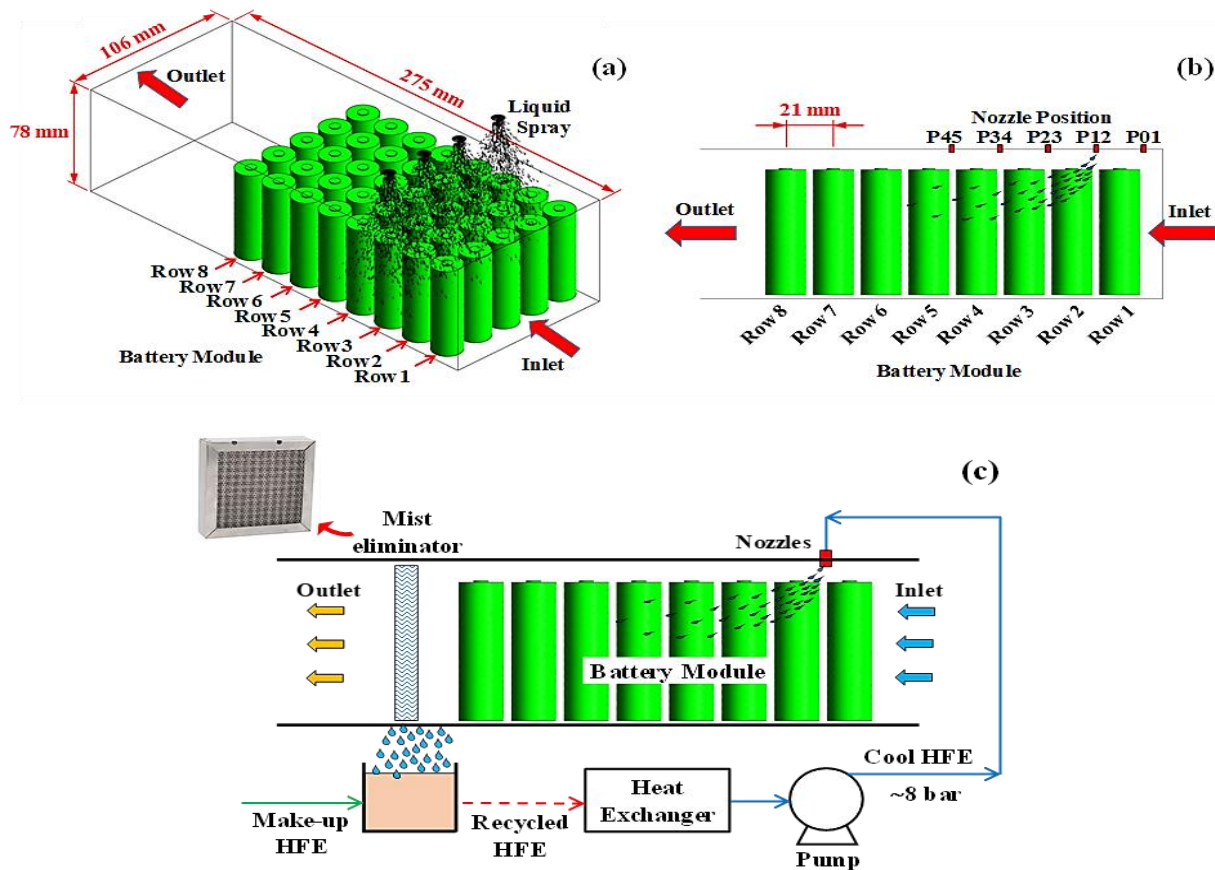

Fig. 1 (a) Schematic diagram of the battery module and its cooling system; (b) Position of nozzles; (c) Conceptual diagram of the HFE recirculation system.

Table 1. Specifications and thermal properties of Panasonic NCR18650B battery.

Characteristics	Value	
Cell length	65 mm	
Cell diameter	18 mm	
Anode material	Graphite	
Cathode material	$LiNi_{0.8}Co_{0.15}Al_{0.05}O_2$	
Electrolyte material	$LiPF_6$ in EC-DMC-DEC	
Nominal capacity	Min. 3250 mAh	
	Typ. 3350 mAh	
Charging	CC-CV, Std. 1625 mA, 4.2 V, 4.0 hrs.	
	Max. Discharge Rate 2C	
	Max. Discharge Rate 2C	
Nominal voltage	3.6 V	
Weight (max)	48.5 g	
Temperature	Charge: 0 to +45 °C @ 0.3C-rate	
	Discharge: -20 to +60 °C @ 1C-rate	
	Storage: -20 to +50 °C	
Energy density (based on bare cell)	Volumetric: 676 Wh/L	
	Gravimetric: 243 Wh/kg	
Anisotropic thermal conductivities	radial directions, kr	0.951 W/m-°C[7]
	axial direction, kZ	37.106 W/m-°C[7]
	tangential direction, kφ	37.106 W/m-°C[7]
Density, ρ	3,602.12 kg/m3[7]	
Specific heat capacity, cp	776.59 J/kg-°C[7]	

Table 2. Product information of 3M™ Novec™ Engineered Fluid HFE-7100.[35]

Properties	Value
Formula	$C_4F_9OCH_3$
Molecular weight	250
Boiling point	61 °C
Freezing point	-135 °C
Density, ρ	1,510 kg/m^3
Specific heat capacity, c_p	1,183 J/kg-°C
Thermal conductivity, k	0.069 W/m-°C
Viscosity, μ	1.168×10^{-3} Pa-s
Latent heat of vaporization	112 kJ/kg
Liquid surface tension	13.6 mN/m

eliminator would be installed. This device would use several compressed layers of knitted wire mesh to capture the droplets from a vapor stream through a series of three stages: collision & adherence to the wire surfaces, coalescence into larger droplets, and drainage from the mist eliminator pad as a separate stream. The separated HFE would then be blended with the stored liquid HFE and cooled by heat exchanger before being recirculated in the system. The proposed recirculation process of the HFE is shown schematically in Fig. 1(c).

3. Heat generation of battery

Before carrying out simulations to evaluate the performance of the cooling system, it is necessary to discuss the heat generated in a battery. There are four main sources of heat generation during the charging/discharging process, which are: reversible heat due to entropy change of the reaction, irreversible heat due to ohmic loss, heat due to side reactions and heat due to mixing.[36-38] The reversible heat can be positive (released) or negative (absorbed) depending on whether the battery is "discharging" or "charging". This heat is generated from the reversible entropy change during the electrochemical reaction at the cathode and anode. The entropic heat absorbed or released in the forward reaction is equal to the amount of heat released or absorbed in the backward reaction. From thermodynamics, the entropy change during the electrochemical reaction is related to the open circuit potential (U_{OC}), and the entropic heat can be expressed through the following relation:

$$\dot{Q}_{rev} = I\left(T\frac{dU_{OC}}{dT}\right) \tag{1}$$

where I is the current (positive on discharge) of the battery cell, T is the absolute temperature and dU_{OC}/dT is the entropic heat coefficient.

Irreversible heat generation is caused by the potential drop due to electron transport resistance during the electrochemical reactions in the electrodes, electrolyte, and current collector. Thus, the irreversible heat generation is an exothermic process and strongly depends on charge/discharge current. The rate of irreversible heat generation is given as:

$$\dot{Q}_{irr} = I(U_{OC} - U) = I^2R \tag{2}$$

where U_{OC} is the open-circuit voltage, U is the battery voltage, and R is the internal resistance of the cell.

At high temperatures, additional reactions occur between the cell materials, including the solid electrolyte interphase (SEI) decomposition, electrolyte-anode reaction, electrolyte-cathode reaction, and electrolyte-binder decomposition. The total heat source due to side reactions can be expressed as:

$$\dot{Q}_{sr} = \dot{Q}_{SEI} + \dot{Q}_{an} + \dot{Q}_{ca} + \dot{Q}_e = \sum_k H_k m_k R_k \tag{3}$$

where H_k, m_k and R_k are the reaction enthalpy, mass and

reaction rate of the chemical reaction k, respectively. All of these series reactions are exothermic. The kinetics of each reaction can be found in.[39,40] Heat generated due to side reactions increases exponentially at high temperatures and may lead to thermal runaway. However, at lower temperatures, the rates of side reactions are typically slow. As a result, the heat source due to side reactions can be ignored at operating temperatures below 80 °C.[38]

The heat generated by mixing is the enthalpy change when non-reactive substances are blended together. The impact of concentration gradients on this loss is significant. It can be released or absorbed as a result of the formation and relaxation of the concentration gradients in the electrolyte and the cathode particles during the operation of the battery. The heat of mixing can be expressed as:

$$\dot{Q}_{mix} = \frac{\partial}{\partial t}\left[\frac{1}{2}\frac{\partial H_S}{\partial c_S}\int(c_S - c_{S,\infty})^2 dV\right] \qquad (4)$$

where $\partial H_S/\partial c_S$, c_S and $c_{S,\infty}$ are the change in enthalpy of mixing for the species, the local and volume-averaged concentrations of the species, respectively. At low charge/discharge rates where the diffusion rate is comparable to the lithium inflow/outflow rate, strong concentration gradients do not develop. Therefore, the rate of enthalpy change due to mixing is relatively low compared to that due to the electron transfer reaction. At high charge/discharge rates, lithium flux propagates through a strong concentration gradient, leading to a significant enthalpy change. Therefore, the heat of mixing cannot be disregarded during high charge/discharge rates.[41] Hence, the total heat generated in the battery consisting of the four different sources can be rewritten as:

$$\dot{Q}_{gen} = IT\frac{dU_{OC}}{dT} + I^2R + \sum_k H_k m_k R_k +$$

$$\frac{\partial}{\partial t}\left[\frac{1}{2}\frac{\partial H_S}{\partial c_S}\int(c_S - c_{S,\infty})^2 dV\right] \qquad (5)$$

The first term on the right side is the reversible heat due to entropic change. The entropic heat coefficient (dU_{OC}/dT) which is a function of the state of charge (SOC) can be determined from the experimental results as shown in Fig. 2. The second term is the irreversible heat due to ohmic loss. The internal resistance (R), which is composed of the ohmic and polarization resistances, is dependent on both the temperature and SOC of the battery as presented in Fig. 2. The reversible heat is important at all C-rates, particularly at low C-rate, while the irreversible heat dominates at high C-rate.[42] The third term is the heat due to side chemical reactions. It becomes more prominent at high temperatures. The last term is the heat due to mixing that is quite small compared with the other heat sources. However, heat due to mixing is cited as a

significant contributor to heat generation of battery at high charge/discharge rate.

In this work, the complex components of a small battery, including the positive and negative electrodes, separators, and current collectors, are simplified using a homogeneous structure with an anisotropic thermal conductivity. Spatial variation in SOC and heat from mixing and side reactions are neglected, since their contributions are small in normal operating conditions of small lithium batteries. Therefore, the sources of heat generation considered in this battery model are entropic heat and resistive heat.

$$\dot{Q}_{gen} = IT\frac{dU_{OC}}{dT} + I^2R \qquad (6)$$

4. Governing equations and simulation method

A three-dimensional model for transient simulation of the battery module is executed using the commercial CFD software, ANSYS Fluent. For the liquid spray cooling of the battery module, the two-phase flow behavior in which the small liquid droplets are suspended in the air stream is characterized by the Eulerian-Eulerian approach. Both air and liquid HFE droplets are treated as interpenetrating continua. In each control volume, a gaseous phase, consisting of air and HFE vapor, and a liquid phase consisting of various-sized HFE droplets exist. Due to the presence of two phases in the continuum, the transports of mass and momentum have to be weighted by the volume fraction of the dispersed phase. The coupling between phases is achieved through the pressure and the interphase exchange coefficients. The set of conservation equations is solved separately for each phase in the Eulerian framework to describe the spray characteristic. The continuity, momentum, and energy equations for phase k are expressed in Ref. [44].

$$\frac{\partial(\alpha_k\rho_k)}{\partial t} + \nabla\cdot(\alpha_k\rho_k\vec{v}_k) = \sum_{l=1,l\neq k}^n \Gamma_{kl} \qquad (7)$$

$$\frac{\partial(\alpha_k\rho_k\vec{v}_k)}{\partial t} + \nabla\cdot(\alpha_k\rho_k\vec{v}_k\vec{v}_k) = -\alpha_k\nabla p + \nabla\cdot\alpha_k(\tau_k + \tau_k^t) +$$

$$\alpha_k\rho_k\vec{g} + \sum_{l=1,l\neq k}^n M_{kl} + \vec{v}_k\sum_{l=1,l\neq k}^n \Gamma_{kl} \qquad (8)$$

$$\frac{\partial(\alpha_k\rho_k h_k)}{\partial t} + \nabla\cdot(\alpha_k\rho_k\vec{v}_k h_k) = \nabla\cdot\alpha_k(q_k + q_k^t) + \alpha_k\rho_k\vec{g}\cdot$$

$$\vec{v}_k + \nabla\cdot\alpha_k(\tau_k + \tau_k^t)\cdot\vec{v}_k + \alpha_k\frac{\partial p}{\partial t} + \sum_{l=1,l\neq k}^n H_{kl} +$$

$$h_k\sum_{l=1,l\neq k}^n \Gamma_{kl} \qquad (9)$$

where Γ_{kl} is the mass transfer source term due to droplet breakup, collisions and evaporation, M_{kl} is the interfacial momentum transfer source term (two-way coupling), and H_{kl} is the energy exchange source term between phases k and l.

In this work, a uniform droplet size distribution of 10 μm is assumed as the initial spray characteristic, and the dispersed
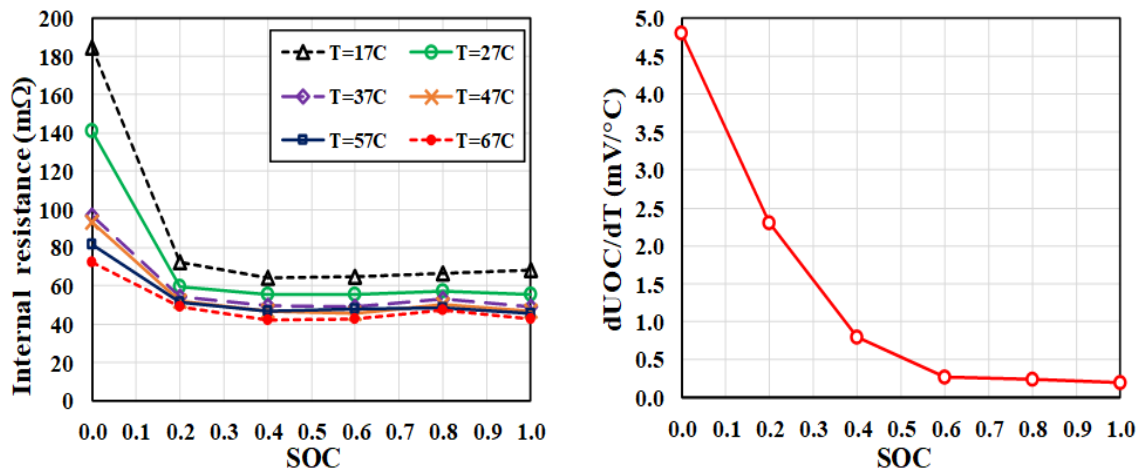
Fig. 2 Experimental data for the internal resistance and entropy thermal coefficient of battery.[43]

phase is dilute enough to ignore droplet collisions. The drag function of Schiller and Naumann and the lift model of Saffmen-Mei are applied for the momentum exchange coefficients. The Ranz-Marshall correlation is used for the heat transfer coefficient of droplets. These terms contain the appropriate physics of the spray model, and further details can be found in Ref. [44,45]. As a requirement of the conservative condition, the sum of all phasic volume fractions must equal 1:

$$\alpha_g + \sum_{k=2}^{n_{droplets}} \alpha_k = 1 \qquad (10)$$

where α_g is the volume fraction of gas phase containing air and HFE vapor, and the liquid phase consists of the droplets of various sizes. Since air and HFE vapor are mixed in the gas phase, another transport equation for individual substance is required.[46]

$$\frac{\partial(\alpha_g \rho_g Y_i)}{\partial t} + \nabla \cdot (\alpha_g \rho_g \vec{v}_g Y_k) =$$

$$\nabla \cdot \left(\alpha_g \left(\rho_g D_{Y_i} + \frac{\mu_g^t}{Sc^t} \right) \nabla Y_i \right) + S_{Y_i} \qquad (11)$$

where Y_i is the mass fraction for substance i, and S_{Y_i} is the source term of the evaporated liquid mass from the droplets.

The heat source for the battery module can be found by Eq. (6), and the governing equation for heat conduction in each battery can be written as:[7]

$$\rho_b c_{p,b} \frac{\partial T_b}{\partial t} = \frac{k_{b,r}}{r} \frac{\partial}{\partial r}\left(r \frac{\partial T_b}{\partial r} \right) + \frac{k_{b,\theta}}{r^2} \frac{\partial^2 T_b}{\partial \theta^2} + k_{b,z} \frac{\partial^2 T_b}{\partial z^2} + \dot{Q}_{gen}$$

$$(12)$$

The heat generation rate of the battery is loaded by coding the User Define Function (UDF). Phase Coupled SIMPLE scheme is used for pressure-velocity coupling of the two-phase flow and Presto scheme is used for pressure discretization. Second-order upwind scheme is selected to discretize all the governing equations and turbulent flow model involved. Realizable $k-\varepsilon$ turbulent model[47] is selected to capture the flow field of the mixture. The near-wall region solved using enhanced wall treatment, requiring the y+ of the boundary layer meshes around unity. The thickness of the first layer mesh near the wall is about 0.1 mm. The meshed geometry discretized with tetrahedral elements is shown in Fig. 3, where the inflation layers and differences in mesh sizing for different regions are apparent.

Initially, the system is at an ambient temperature of 27 °C. Air is induced at the inlet boundary with a uniform velocity of
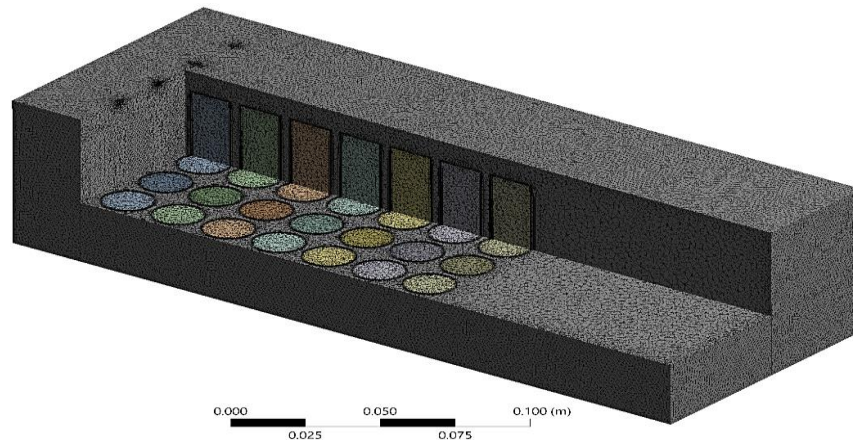

Fig. 3 Meshed model of the BTMS.

2 m/s and a temperature of 27 °C. Monodispersed HFE-7100 droplets are injected at the inlet boundary with a constant velocity and a temperature of 25 °C. The pressure-outlet boundary condition is assigned to the outlet. A no-slip boundary condition is imposed on all walls, and the effects of wall adhesion are accounted for by the given contact angle of 90°. The enclosure walls are considered to be thermally adiabatic. The battery wall/fluid interface is assumed to have a coupled thermal boundary, which means that both temperature and heat flux are continuous at the interface.

5. Results and discussion

In the simulation, a fully charged battery module ($SOC = 1$) was continuously discharged at 2C-rate until it was completely depleted ($SOC = 0$), which was achieved by using a constant discharge current of 6.8 Amps for approximately 30 minutes. The HFE was sprayed vertically downward from the nozzles while ambient air with a velocity of 2 m/s was induced horizontally across the falling HFE droplets as shown in Fig. 1. By the HFE droplets and ambient air flowing together, the convective heat transfer was enhanced and thereby led to an improvement in the cooling performance of the battery module. The objective of designing the thermal management system is to maintain a maximum cell temperature under 40 °C and to keep the temperature uniformity within 5 °C, so as to avoid a decrease in charging efficiency and battery life.

Before conducting the simulation, the mesh independence and time step studies were carried out to ensure that the generated mesh and time step size were appropriate for capturing the flow and thermal characteristics of the system. During sensitivity analysis, the boundary and initial condition remain the same. Different sizes of element were generated, ranging from coarse to dense, to analyze grid-independence of the model as shown by the results in Fig. 4. Once the number of elements reached 4,667,630, the temperatures of the battery module stabilized and remained relatively unchanged. Similarly, the sensitivity analysis was also conducted for time steps, as shown in Fig. 4. There were small changes in cell temperatures for time steps less than 10 seconds. To avoid further longer computational time and resource usage, the model with 4,667,630 elements and a time step of 10 seconds was discretized for subsequent simulations, where the simulated maximum cell temperature error will not exceed the limit of 0.17 °C.

Figure 5 displays the temperature development in each row of the battery module during discharge. The HFE liquid was injected from nozzles at position P01, where the nozzles were located at the front of the battery module as shown in Fig. 1. The cell temperature increased linearly in the beginning of the discharge and then slowed down in the middle stage. This was because the air was heated as it passed through the rows of cells, thus causing the temperature difference to drive the convective heat transfer. The small increase in cell row temperature allowed the temperature difference to be restored, so that there was almost an equilibrium between heat generated and convective cooling. In the final stage of discharge, the battery temperature rose rapidly due to the increased entropy thermal coefficient and internal resistance at lower SOC, as presented in Fig. 2, resulting in a higher heat generation rate. The average temperatures of batteries in each row increased along the horizontal air flow path, with the exception of the first row near the nozzles. This was likely due to the increased free-stream turbulence from the preceding rows and the shear effects from the constriction of the flow passages. Wakes were formed and trapped between the neighboring rows of batteries. This enhanced heat transfer in subsequent rows, and this increase in heat transfer persisted until the third row. Then, the heat transfer became stable from
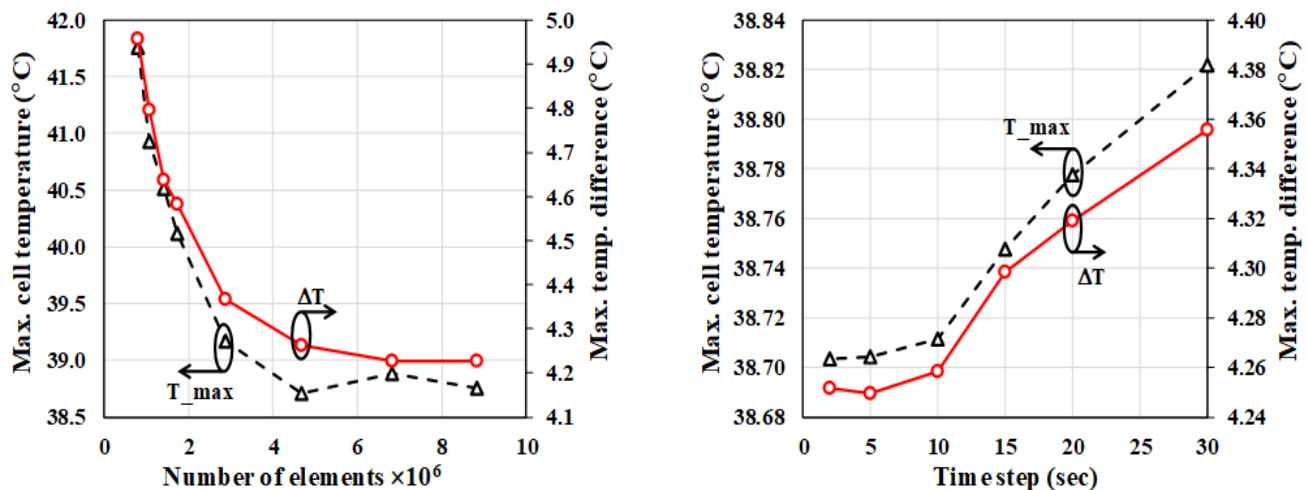

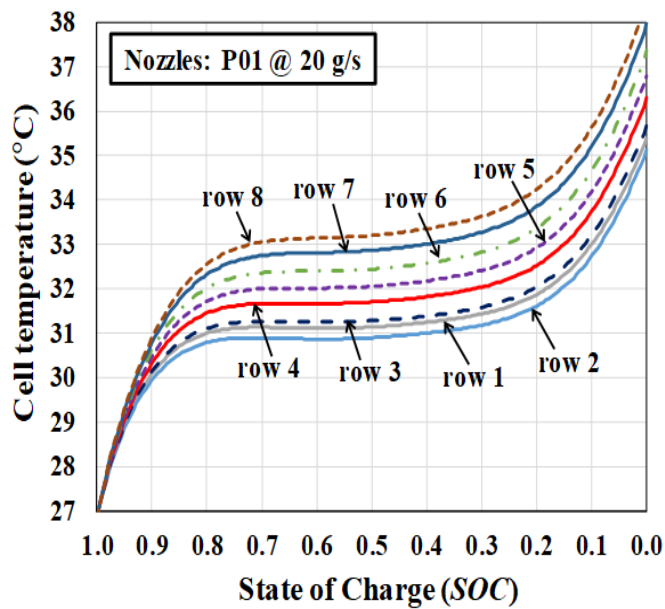**Fig. 4** Mesh independence and time step studies.

Fig. 5 Temperature evolution of the battery module for 2C discharge rate.

the fourth row on.[7] Additionally, the reduced contact of HFE droplets with the cell surfaces in the frontmost row near the nozzles reduced the effective wetted surface area for convective heat transfer.

Figure 6 shows the motion of HFE droplet along the flow channel, with color representing the volume fraction of HFE liquid at the end of discharge process. Due to fine monodispersed spray, the droplets likely completed evaporation within a short distance, as evidenced by the volume fraction of HFE liquid. This is due to the high specific surface area of the fine droplets, which creates strong heat convection between the droplets and surrounding air, leading to complete evaporation. Moreover, the trajectories of droplets colored by velocity streamline, as shown in Fig. 7, also affect the cell temperature. HFE droplets absorbing heat from the cell surface as they impinge and then being carried away by

airflow causes a sharp decrease in surface temperature in the impingement zone due to the high heat transfer coefficient of liquid droplets. Besides, the droplets with a higher flow rate can penetrate deeper into the battery module. On the other hand, the low-velocity HFE spray Fig. 7(a) shows minimal impact on the cooling rate of the battery module, as most HFE droplets are swept away by cooling air before absorbing heat from the warm battery surface.
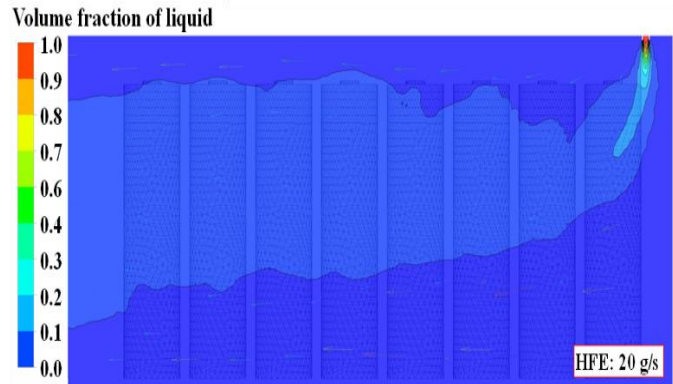

Fig. 6 The propagation of HFE droplets through the battery.

The effect of the HFE injection position on the cooling performance of the battery module was also investigated and the results are presented in Fig. 8. As the position of nozzles was altered as shown schematically in Fig. 1(b), the total HFE flow rate was kept constant at 20 g/s. At the end of discharge, the maximum cell temperatures at all injection points remained below 40 °C, and the nozzle at P12 provided the lowest maximum temperature. Furthermore, the maximum temperature differences of the battery module of all injection points, except at location P01, were less than 5 °C. Although the lowest average cell temperature was found at the nozzle location P01, the last row of the battery module had a higher temperature, resulting in a larger temperature difference that exceeded the recommended range. For a dry air-cooling
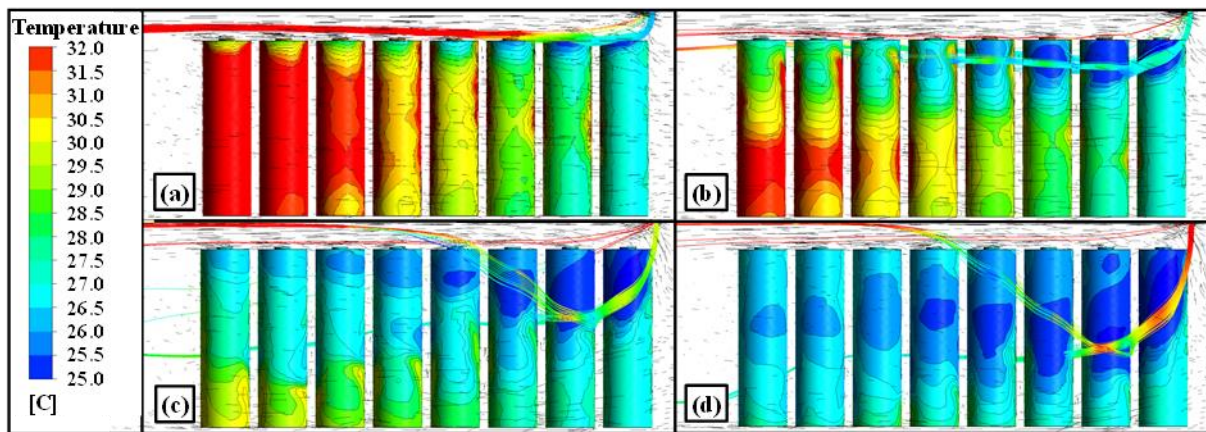

Fig. 7 Temperature contours of the battery module and HFE streamlines for different HFE injection rates: *(a)* 10 g/s, *(b)* 20 g/s, *(c)* 40 g/s, *(d)* 60 g/s.
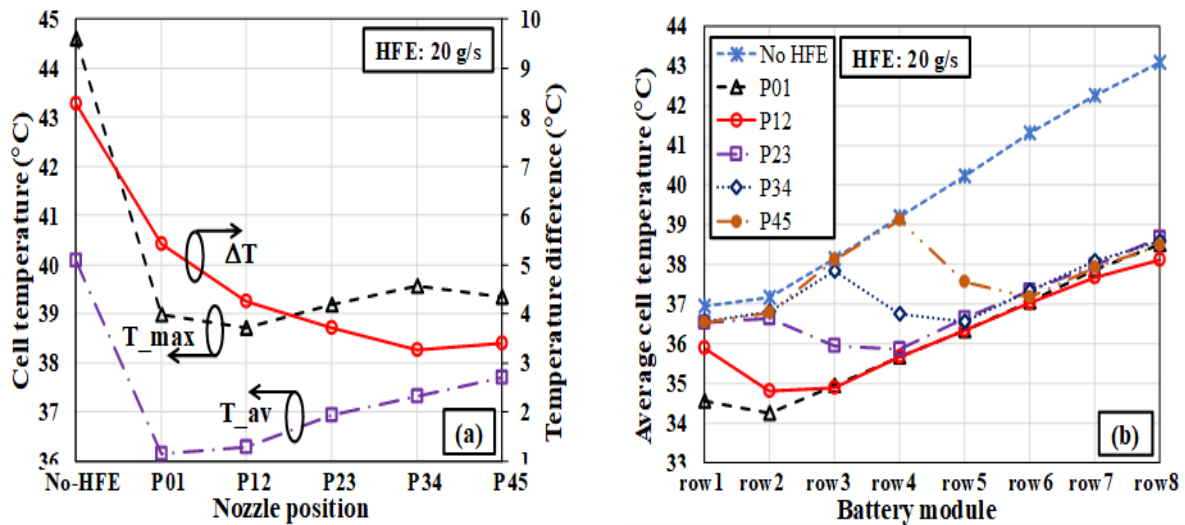
Fig. 8 Impact of nozzle position on the temperature distribution of the battery module.

system, both the maximum temperature and temperature difference are higher than the thermal requirements in the BTMS design. Therefore, the HFE spray cooling can enhance the performance of the air-cooling system, and the arrangement of nozzles has a significant impact on the heat dissipation rate of the hybrid cooling system.

Increasing the amount of HFE injection improved the heat dissipation rate of the system, as seen by the decreasing cell temperatures at a slower rate in Fig. 9. As a result, the maximum temperature difference across the battery module decreased exponentially. For proper battery operation, the HFE mass flow rate should be at least 20 g/s. Excessive increases in HFE flow rate have limited impact on cell temperature reduction, indicating that excessive HFE injection in the hybrid cooling system is not cost-effective for heat dissipation.

That the layout of the nozzle and the amount of HFE injection play a significant role in cooling the battery module has been discussed, but excessive HFE can be detrimental to efficiency and cost. Therefore, it is necessary to determine the optimal design of the HFE spray. To evaluate these optimal conditions, a parameter called the *spray cooling effect* has been defined. This parameter is the ratio of the heat dissipation rate augmented by liquid spray to the mass flow rate of the liquid spray.

$$\text{Spray cooling effect (J/g)} = \frac{\text{Heat dissipation rate of battery module (J/s)}}{\text{Mass flow rate of HFE injected (g/s)}}$$

(13)

To find the optimum amount of HFE and placement of nozzles, extensive simulations are executed for different nozzle positions (*i.e.* P01, P12, P23, P34, and P45) and for different HFE flow rates (*i.e.* 0, 5, 10, 20, 30, 40, 50, and 60 g/s). Fig. 10 displays the spray cooling effect for different combinations
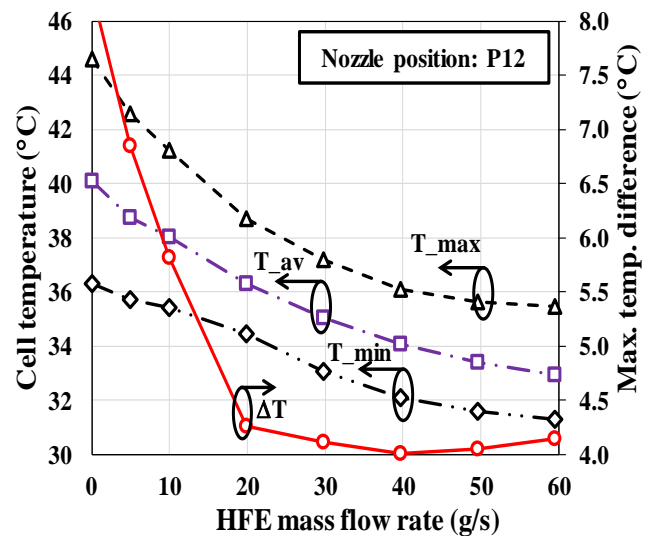

Fig. 9 Impact of HFE flow rate on the temperature distribution of the battery module.

of nozzle arrangements and injection rates. The design constraints are depicted by the dashed lines in the figure, which are $T_{max} > 40\ °C$ in the diagonal line zone, and $\Delta T > 5\ °C$ in the red polka dot zones. Increasing the mass flow rate of HFE weakens the spray cooling effect because there is excess HFE for dissipating limited heat. This overcooling causes the unnecessary expenditure of energy. Moreover, placing nozzles farther from the inlet also diminishes the spray cooling effect. This is because some HFE is swept away by air stream before absorbing heat from the batteries. Therefore, the highest spray cooling effect is found in the lower left part of the domain, but this design is completely unacceptable as it exists in T_{max} failure zone or ΔT failure zone. The optimal design that meets these constraints is shown to be where the HFE nozzles are at position P12 with a flow rate of 20 g/s. If the flow rate of the liquid spray were to decrease to a certain

level, *e.g.* 15 g/s, the maximum cell temperature would increase significantly, thereby increasing the risk of thermal runaway in the battery. Hence, the diagram in Fig. 10 can be used as a guide for determining the optimal design of the spray-assisted forced-air cooling system for the battery module.
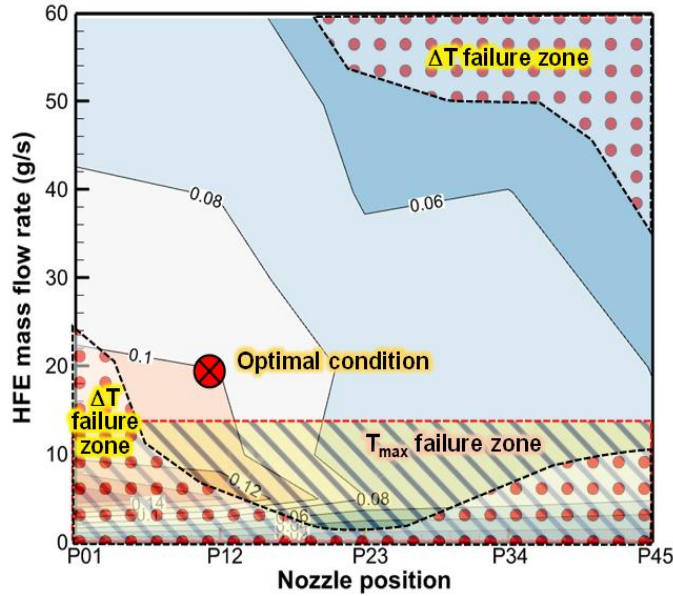

Fig. 10 Contour plot of spray cooling effect versus nozzle position and HFE flow rate.

6. Conclusions

In this study, the heat dissipation characteristics of Li-ion batteries when subjected to forced-air cooling combined with liquid spray were numerically analyzed. The non-conductive liquid, Novec fluid HFE-7100, was used in the form of uniformly sized droplets injected into a dry air stream to enhance convective heat transfer. The following conclusions were made:

(1)   Due to the formation of fine droplets, a large amount of liquid spray evaporates rapidly over a short distance from the nozzles, causing a significant decrease in the volume fraction of the liquid. This evaporation process absorbs heat energy from the surroundings, thereby enhancing the heat transfer capability of the cooling medium. The remaining droplets dispersed in the airflow and deposited on the cell surfaces also absorb heat from their surroundings.

(2)   During the discharge process, the temperature of the battery cells significantly increases in the *SOC* range of 0–0.2. This is due to the high rate of heat generation caused by the battery characteristics, particularly its internal resistance. This range of SOC is considered dangerous for the battery as high temperatures can decrease its capacity.

(3)   Using the spray-assisted forced-air cooling system results

in a more uniform temperature distribution of the battery module compared to that when using dry air cooling alone. With the optimal design, the maximum temperature and temperature uniformity can be reduced 5.89 °C and 4.02 °C, respectively, compared to dry air cooling.

(4)   Increasing the amount of liquid spray improves the heat transfer capability of the system. To ensure that the battery operates within the optimum temperature range, it is recommended to maintain a minimum HFE injection rate of 20 g/s. However, the ability to decrease cell temperature decreases gradually as the amount of HFE liquid spray increases.

(5)   To achieve maximum cooling performance, it is crucial to ensure that the liquid jet trajectory contacts the cell surface, as the high heat transfer coefficient of the droplets facilitates efficient heat dissipation. The optimal design is achieved when the nozzles are mounted between rows 1 and 2 of the battery module.

Future research should focus on validating the accuracy and practicality of the model by comparing the results with those obtained from experiments.

Conflict of Interest

There is no conflict of interest.

Supporting Information

Not applicable.

Nomenclature

Symbols	Description
c	concentration [mol/m^3]
c_p	specific heat capacity [J/kg–°C]
D	effective diffusion coefficient
g	body force vector [N/m^3]
h	specific enthalpy [J/kg]
H	reaction enthalpy [J/kg]
H_{kl}	enthalpy exchange term [W/m^3]
I	discharge/charge current [A]
k	thermal conductivity [W/m–°C]

m	mass [kg]		HFE	Hydrofluoroether
M_{kl}	momentum exchange term [W/m^3]		LIB	Lithium-ion battery
p	pressure [Pa]		LiPF6	lithium hexafluorophosphate
$\dot{Q}$	heat generation rate [W]		OC	Open circuit
R	reaction rate [s^{-1}]		PCM	Phase change material
R	internal resistance [Ω]		SEI	Solid electrolyte interphase
Sc^t	turbulent Schmidt number [–]		SOC	State of Charge

t	time [s]
T	temperature [°C]
T_{max}	maximum cell temperature [°C]
ΔT	temperature difference within
U	voltage [V]
$\bar{v}$	velocity [m/s]
V	volume [m^3]
Y	mass fraction [–]

Greeks	
μ	dynamic viscosity [kg/m-s]
τ	shear stress [N/m^2]
Γ	mass exchange term [kg/(m^3-s)]
α	volume fraction [–]
ρ	density [kg/m^3]

Subscripts	
b	battery
c	cell
f	fluid
g	gas phase
gen	generation
i	substance
k	phase, species
kl	between phase k and l
mix	mixing
rev	reversible
irr	irreversible
S	species

Abbreviatio	
BTMS	Battery thermal management
C-rate	Charge/Discharge rate
EC	ethylene carbonate
EV	Electric vehicle
DEC	diethyl carbonate
DMC	dimethyl carbonate

References

[1] F. Leng, C. M. Tan, M. Pecht, Effect of Temperature on the Aging rate of Li Ion Battery Operating above Room Temperature, *Scientific Reports*, 2015, **5**, 12967, doi: 10.1038/srep12967.

[2] Q. Wang, J. Sun, X. Yao, C. Chen, Thermal Behavior of Lithiated Graphite with Electrolyte in Lithium-Ion Batteries, *Journal of The Electrochemical Society*, 2006, **153**, A329, doi: 10.1149/1.2139955.

[3] M. Malik, I. Dincer, M. Rosen, M. Fowler, Experimental Investigation of a New Passive Thermal Management System for a Li-Ion Battery Pack Using Phase Change Composite Material, *Electrochimica Acta*, 2017, **257**, 345-355, doi: 10.1016/j.electacta.2017.10.051.

[4] O. Kalaf, D. Solyali, M. Asmael, Q. Zeeshan, B. Safaei, A. Askir, Experimental and simulation study of liquid coolant battery thermal management system for electric vehicles: A review, *International Journal of Energy Research*, 2021, **45**, 6495-6517, doi: 10.1002/er.6268.

[5] G. M. Cavalheiro, T. Iriyama, G. J. Nelson, S. Huang, G. Zhang, Effects of Nonuniform Temperature Distribution on Degradation of Lithium-Ion Batteries, *Journal of Electrochemical Energy Conversion and Storage*, 2020, **17**, 021101, doi: 10.1115/1.4045205.

[6] L. H. Saw, Y. Ye, A. A. O. Tay, W. T. Chong, S. H. Kuan, M. C. Yew, Computational fluid dynamic and thermal analysis of Lithium-ion battery pack with air cooling, *Applied Energy*, 2016, **177**, 783-792, doi: 10.1016/j.apenergy.2016.05.122.

[7] P. Saechan, I. Dhuchakallaya, Numerical investigation of air cooling system for a densely packed battery to enhance the cooling performance through cell arrangement strategy, *International Journal of Energy Research*, 2022, **46**, 20670-20684, doi: 10.1002/er.7571.

[8] Y. Xie, Y. Liu, M. Fowler, M.-K. Tran, S. Panchal, W. Li, Y. Zhang, Enhanced optimization algorithm for the structural design of an air-cooled battery pack considering battery lifespan and consistency, *International Journal of Energy Research*, 2022, **46**, 24021-24044, doi: 10.1002/er.8700.

[9] S. Park, D. Jung, Battery cell arrangement and heat transfer fluid effects on the parasitic power consumption and the cell temperature distribution in a hybrid electric vehicle, *Journal of Power Sources*, 2013, **227**, 191-198, doi: 10.1016/j.jpowsour.2012.11.039.

[10] T. Wang, K. J. Tseng, J. Zhao, Z. Wei, Thermal investigation of lithium-ion battery module with different cell arrangement

structures and forced air-cooling strategies, *Applied Energy*, 2014, **134**, 229-238, doi: 10.1016/j.apenergy.2014.08.013.

[11] E. Jiaqiang, M. Yue, J. Chen, H. Zhu, Y. Deng, Y. Zhu, F. Zhang, M. Wen, B. Zhang, S. Kang, Effects of the different air cooling strategies on cooling performance of a lithium-ion battery module with baffle, *Applied Thermal Engineering*, 2018, **144**, 231-241, doi: 10.1016/j.applthermaleng.2018.08.064.

[12] H. Xu, X. Zhang, G. Xiang, H. Li, Optimization of liquid cooling and heat dissipation system of lithium-ion battery packs of automobile, *Case Studies in Thermal Engineering*, 2021, **26**, 101012, doi: 10.1016/j.csite.2021.101012.

[13] R. Gao, Z. Fan, S. Liu, A gradient channel-based novel design of liquid-cooled battery thermal management system for thermal uniformity improvement, *Journal of Energy Storage*, 2022, **48**, 104014, doi: 10.1016/j.est.2022.104014.

[14] A. Sarchami, M. Tousi, M. Kiani, A. Arshadi, M. Najafi, M. Darab, E. Houshfar, A novel nanofluid cooling system for modular lithium-ion battery thermal management based on wavy/stair channels, *International Journal of Thermal Sciences*, 2022, **182**, 107823, doi: 10.1016/j.ijthermalsci.2022.107823.

[15] S. Wu, L. Lao, L. Wu, L. Liu, C. Lin, Q. Zhang, Effect analysis on integration efficiency and safety performance of a battery thermal management system based on direct contact liquid cooling, *Applied Thermal Engineering*, 2022, **201**, 117788, doi: 10.1016/j.applthermaleng.2021.117788.

[16] Y. Li, Z. Zhou, L. Hu, M. Bai, L. Gao, Y. Li, X. Liu, Y. Li, Y. Song, Experimental studies of liquid immersion cooling for 18650 lithium-ion battery under different discharging conditions, *Case Studies in Thermal Engineering*, 2022, **34**, 102034, doi: 10.1016/j.csite.2022.102034.

[17] C. Liu, D. Xu, J. Weng, S. Zhou, W. Li, Y. Wan, S. Jiang, D. Zhou, J. Wang, Q. Huang, Phase Change Materials Application in Battery Thermal Management System: A Review, *Materials*, 2020, **13**, 4622, doi: 10.3390/ma13204622.

[18] Z. Ling, Z. Zhang, G. Shi, X. Fang, L. Wang, X. Gao, Y. Fang, T. Xu, S. Wang, X. Liu, Review on thermal management systems using phase change materials for electronic components, Li-ion batteries and photovoltaic modules, *Renewable and Sustainable Energy Reviews*, 2014, **31**, 427-438, doi: 10.1016/j.rser.2013.12.017.

[19] Z. Ling, F. Wang, X. Fang, X. Gao, Z. Zhang, A hybrid thermal management system for lithium ion batteries combining phase change materials with forced-air cooling, *Applied Energy*, 2015, **148**, 403-409, doi: 10.1016/j.apenergy.2015.03.080.

[20] C.-V. Hémery, F. Pra, J.-F. Robin, P. Marty, Experimental performances of a battery thermal management system using a phase change material, *Journal of Power Sources*, 2014, **270**, 349-358, doi: 10.1016/j.jpowsour.2014.07.147.

[21] Q. Huang, X. Li, G. Zhang, J. Zhang, F. He, Y. Li, Experimental investigation of the thermal performance of heat pipe assisted phase change material for battery thermal management system, *Applied Thermal Engineering*, 2018, **141**, 1092-1100, doi: 10.1016/j.applthermaleng.2018.06.048.

[22] H. N. Khaboshan, F. Jaliliantabar, A. A. Abdullah, S. Panchal, Improving the cooling performance of cylindrical

lithium-ion battery using three passive methods in a battery thermal management system, *Applied Thermal Engineering*, 2023, **227**, 120320, doi: 10.1016/j.applthermaleng.2023.120320.

[23] A. Alkhedhair, H. Gurgenci, I. Jahn, Z. Guan, S. He, Numerical simulation of water spray for pre-cooling of inlet air in natural draft dry cooling towers, *Applied Thermal Engineering*, 2013, **61**, 416-424, doi: 10.1016/j.applthermaleng.2013.08.012.

[24] J. Tissot, P. Boulet, F. Trinquet, L. Fournaison, H. Macchi-Tejeda, Air cooling by evaporating droplets in the upward flow of a condenser, *International Journal of Thermal Sciences*, 2011, **50**, 2122-2131, doi: 10.1016/j.ijthermalsci.2011.06.004.

[25] H. Montazeri, B. Blocken, J. L. M. Hensen, CFD analysis of the impact of physical parameters on evaporative cooling by a mist spray system, *Applied Thermal Engineering*, 2015, **75**, 608-622, doi: 10.1016/j.applthermaleng.2014.09.078.

[26] H. Yang, L. Rong, X. Liu, L. Liu, M. Fan, N. Pei, Experimental research on spray evaporative cooling system applied to air-cooled chiller condenser, *Energy Reports*, 2020, **6**, 906-913, doi: 10.1016/j.egyr.2020.04.001.

[27] Y. Yang, L. Yang, X. Du, Y. Yang, Pre-cooling of air by water spray evaporation to improve thermal performance of lithium battery pack, *Applied Thermal Engineering*, 2019, **163**, 114401, doi: 10.1016/j.applthermaleng.2019.114401.

[28] L. H. Saw, H. M. Poon, H. S. Thiam, Z. Cai, W. T. Chong, N. A. Pambudi, Y. J. King, Novel thermal management system using mist cooling for lithium-ion battery packs, *Applied Energy*, 2018, **223**, 146-158, doi: 10.1016/j.apenergy.2018.04.042.

[29] R. Zhao, J. Liu, J. Gu, L. Zhai, F. Ma, Experimental study of a direct evaporative cooling approach for Li-ion battery thermal management, *International Journal of Energy Research*, 2020, **44**, 6660-6673, doi: 10.1002/er.5402.

[30] R. Youssef, M. S. Hosen, J. He, J. Jaguemont, L. D. Sutter, J. V. Mierlo, M. Berecibar, Effect analysis on performance enhancement of a novel and environmental evaporative cooling system for lithium-ion battery applications, *Journal of Energy Storage*, 2021, **37**, 102475, doi: 10.1016/j.est.2021.102475.

[31] C. M. Barnes, P. E. Tuma, Practical Considerations Relating to Immersion Cooling of Power Electronics in Traction Systems, *IEEE Transactions on Power Electronics*, 2010, **25**, 2478-2485, doi: 10.1109/TPEL.2010.2049864.

[32] R. W. van Gils, D. Danilov, P. H. L. Notten, M. F. M. Speetjens, H. Nijmeijer, Battery thermal management by boiling heat-transfer, *Energy Conversion and Management*, 2014, **79**, 9-17, doi: 10.1016/j.enconman.2013.12.006.

[33] Z. An, L. Jia, X. Li, Y. Ding, Experimental investigation on lithium-ion battery thermal management based on flow boiling in mini-channel, *Applied Thermal Engineering*, 2017, **117**, 534-543, doi: 10.1016/j.applthermaleng.2017.02.053.

[34] I. Mudawar, D. Bharathan, K. Kelly, S. Narumanchi, Two-phase spray cooling of hybrid vehicle electronics, Proceedings of the ITHERM 2008, 11th Intersociety Conference on Thermal and Thermomechanical Phenomena in Electronic Systems. May 28-31, 2008, Orlando, FL, USA. IEEE, 2008, 1210-1221, doi: 10.1109/ITHERM.2008.4544399.

[35] 3M, Technical Data Sheet, Product Information 3M™

Novec™ 7100 Engineered Fluid, 2023, Available: chrome-extension://efaidnbmnnnibpcajpcglclefindmkaj/https://multimedia.3m.com/mws/media/199818O/3m-novec-7100-engineered-fluid.pdf&fn=prodinfo_nvc7100.pdf.

[36] T. M. Bandhauer, S. Garimella, T. F. Fuller, Temperature-dependent electrochemical heat generation in a commercial lithium-ion battery, *Journal of Power Sources*, 2014, **247**, 618-628, doi: 10.1016/j.jpowsour.2013.08.015.

[37] S. Ma, M. Jiang, P. Tao, C. Song, J. Wu, J. Wang, T. Deng, W. Shang, Temperature effect and thermal impact in lithium-ion batteries: A review, *Progress in Natural Science: Materials International*, 2018, **28**, 653-666, doi: 10.1016/j.pnsc.2018.11.002.

[38] Q. Wang, B. Jiang, B. Li, Y. Yan, A critical review of thermal management models and solutions of lithium-ion batteries for the development of pure electric vehicles, *Renewable and Sustainable Energy Reviews*, 2016, **64**, 106-128, doi: 10.1016/j.rser.2016.05.033.

[39] M.-K. Tran, A. Mevawalla, A. Aziz, S. Panchal, Y. Xie, M. Fowler, A Review of Lithium-Ion Battery Thermal Runaway Modeling and Diagnosis Approaches, *Processes*, 2022, **10**, 1192, doi: 10.3390/pr10061192.

[40] J. Chen, D. Ren, H. Hsu, L. Wang, X. He, C. Zhang, X. Feng, M. Ouyang, Investigating the thermal runaway features of lithium-ion batteries using a thermal resistance network model, *Applied Energy*, 2021, **295**, 117038, doi: 10.1016/j.apenergy.2021.117038.

[41] D. Chalise, W. Lu, V. Srinivasan, R. Prasher, Heat of Mixing During Fast Charge/Discharge of a Li-Ion Cell: A Study on NMC523 Cathode, *Journal of the Electrochemical Society*, 2020, **167**, 090560, doi: 10.1149/1945-7111/abaf71.

[42] V. Srinivasan, C. Y. Wang, Analysis of Electrochemical and Thermal Behavior of Li-Ion Cells, *Journal of the Electrochemical Society*, 2003, **150**, A98-A106, doi: 10.1149/1.1526512.

[43] Y. Xie, W. Li, Y. Yang, F. Feng, A novel resistance-based thermal model for lithium-ion batteries, *International Journal of Energy Research*, 2018, **42**, 4481-4498, doi: 10.1002/er.4193.

[44] M. Vujanović, Z. Petranović, W. Edelbauer, J. Baleta, N. Duić, Numerical modelling of diesel spray using the Eulerian multiphase approach, *Energy Conversion and Management*, 2015, **104**, 160-169, doi: 10.1016/j.enconman.2015.03.040.

[45] I. ANSYS, ANSYS Fluent Theory Guide, release 2020 R2, Canonsburg, PA, USA, July 2020.

[46] I. Dhuchakallaya, A. P. Watkins, Auto-ignition of diesel spray using the PDF-Eddy Break-Up model, *Applied Mathematical Modelling*, 2010, **34**, 1732-1745, doi: 10.1016/j.apm.2009.09.019.

[47] T.-H. Shih, W. W. Liou, A. Shabbir, Z. Yang, J. Zhu, A new k-ϵ eddy viscosity model for high Reynolds number turbulent flows, *Computers & Fluids*, 1995, **24**, 227-238, doi: 10.1016/0045-7930(94)00032-t.